COMPARISON OF CONVECTIVE SCHEMES IN HYDROGEN IMPINGING JET CFD SIMULATION

Tolias, I.C.[1] and Venetsanos, A.G.[1]
[1] Environmental Research Laboratory, National Center for Scientific Research Demokritos, Agia Paraskevi, 15310, Greece, tolias@ipta.demokritos.gr, venets@ipta.demokritos.gr

ABSTRACT

Hydrogen impinging jets can be formed in the case of an accidental release indoors or outdoors. The CFD simulation of hydrogen impinging jets suffers from numerical errors resulting in a non-physical velocity and hydrogen concentration field with a butterfly like structure. In order to minimize the numerical errors and to avoid the butterfly effect, high order schemes need to be used. The aim of this work is to give best practices guidelines for hydrogen impinging jet simulations. A number of different numerical schemes is evaluated. The number of cells which discretize the source is also examined.

1.0 INTRODUCTION

Impinging jets have been used extensively in the industry as they offer an effective way to transfer heat and mass. Impinging jets can produce heat transfer coefficients that are up to three times higher at a given maximum flow speed compared to a wall-parallel flow [1]. Typical heat transfer applications include cooling of materials, electronic and turbine components and heating of optical surfaces for defogging. Typical mass transfer application is drying and removal of small surface particulates. Impinging jets can also be appeared as side effects of other applications, such as in the case of a vertical take off or landing system.

Even thought impinging jets have been studied extensively both experimentally and numerically, hydrogen impinging jets have not been examined thoroughly. Hydrogen impinging jets can be formed in various scenarios. Hydrogen vehicles are provided with pressure release device which might be located at the bottom of the storage system. As a result in the case of a release, hydrogen will escape as high momentum jet impinging to the ground. Hydrogen impinging jets can be formed also in the case of an accidental release in closed rooms. Such a case has been studied experimentally in [2] and numerically in [3]. Hydrogen impinging flames have been studied in [4], [5] and [6].

Impinging jets involves complex physics. As we can see in Fig. 1, impinging jets has three distinct main flow regions with distinct flow physics: free jet, stagnation and wall jet. When the flow exits the nozzle, the surrounding fluid entrains into the jet reducing the jet velocity. The mixing region surrounds a core area where the fluid velocity at the centerline is almost equal to the exit velocity. A decaying jet region follows caused by large shear stresses at the jet boundary. In this region, the axial velocity decreases as we move away from the centre forming a Gaussian like profile. This profile becomes wider and shorter as we move away from the nozzle. As the flow approaches the wall, it enters into the stagnation or deceleration region. The axial velocity is rapidly decreased and its direction changes. The static pressure of the flow is increased, transmitting the effect of the wall upstream. High normal and shear stresses are developed due to the non-uniform turning of the flow. Vortices are stretched and turbulence increases. Next, the flow enters into the wall jet region where it moves parallel to the wall. The flow has a shearing layer influenced by both the wall and the velocity gradient with respect to the surrounding stationary fluid. As the flow moves parallel to the wall, the wall jet entrains the surrounding fluid, its thickness grows and its average velocity decreases.

In the case of the hydrogen jet the resulting flow becomes more complex due to the buoyancy. In this paper, we examine numerically the case where a hydrogen jet exits a nozzle at sonic velocity and hits the ground. When the impinging jet hits the ground, a circular velocity field is expected to be formed upon it. The CFD simulation of hydrogen impinging jets suffers from numerical errors resulting in a non-physical velocity and hydrogen concentration field with a butterfly like structure. In order to minimize the numerical errors and to avoid the butterfly effect, high order schemes need to be used.

The aim of this work, is the evaluation of a number of different numerical schemes. The number of cells which discretize the source is also examined.

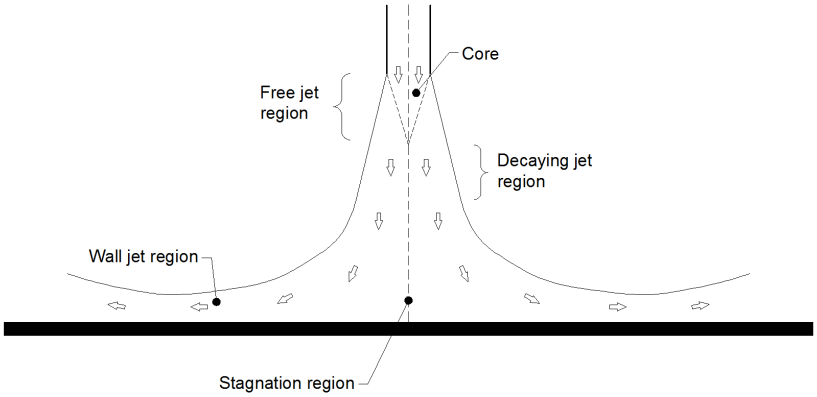

Figure 1. Main flow regions of impinging jet

2.0 MATHEMATICAL METHODOLOGY

For the CFD simulations the ADREA_HF code was used [7]. The code solves the time-averaged Navier-Stokes equations along with the conservation equations of the mass fraction of hydrogen. The multi-component mixture is assumed to be in thermodynamic equilibrium. The equation of state for ideal gases relates pressure with density and temperature. Turbulence is modelled using the standard k-ε model, in which buoyancy effects were included.

2.1 Numerical schemes

In the finite volume method, the differential equations are integrated on computational cells. The values of the variables are stored at the center of the cells (nodes). However, during the discretization process the values of the variables at the cell surfaces are appeared. The calculation of these values is of great importance, especially for the case of the discretization of the convective term of the equations.

We will make use of the following formulation of the convective scheme [8] (Fig. 2):

$$\phi_e = \phi_P + \frac{x_e - x_w}{2}\Psi(R)\left(\frac{\partial\phi}{\partial x}\right)_w \tag{1}$$

where ϕ is the transport quantity (e.g. hydrogen concentration), x is the distance, $\Psi(R)$ is the *limiter* function and r is defined as the gradient ratio:

$$R = \left(\frac{\partial\phi}{\partial x}\right)_e \Big/ \left(\frac{\partial\phi}{\partial x}\right)_w \tag{2}$$

Table 1 presents the numerical schemes that were tested for the current simulations. The schemes have been divided in two categories. The first category includes the k-schemes. These schemes are unbounded, i.e. don't preserve monotony (can produce new extrema to the solution) and as a result they may produce unphysical oscillations to the solution. The second category includes bounded schemes. These schemes are non-linear and they try to combine the high accuracy of the k-schemes with the desirable property of monotony.

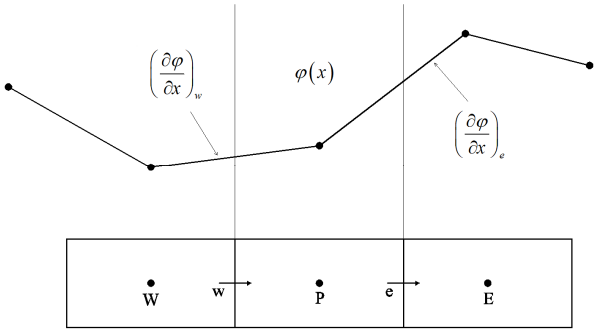

Figure 2. Notation: W, P, E indicate cell nodes, w, e indicate the cell interface and arrows indicate the velocity direction

Table 1. Numerical schemes formulation

Convective Schemes		$\Psi(R)$
k-schemes	**QUICK** [9]	$0.75R+0.25$
	Fromm [10]	$0.5R+0.5$
	Cubic Upwind [11]	$\frac{2}{3}R+\frac{1}{3}$
Bounded schemes	**Upwind**	0
	Minmod [12]	$\max\left(0,\min\left(R,1\right)\right)$
	Van Albada [13]	$\frac{R^2+R}{R^2+1}$
	Van Leer [14][15]	$\frac{\lvert R\rvert+R}{\lvert R\rvert+1}$
	MUSCL [14][15]	$\max\left(0,\min\left(2R,0.5R+0.5,2\right)\right)$
	SMART [16]	$\max\left(0,\min\left(2R,0.75R+0.25,4\right)\right)$
	CHARM [8]	$\frac{R\left(3R+1\right)}{\left(R+1\right)^2}$
	Bounded Central Differences [8]	$\max\left(0,\min\left(R,2\right)\right)$
	Koren-PR [17]	$\frac{2R^2+R}{2R^2-R+2}$
	Spekreijse [8]	$\left(\frac{2}{3}R+\frac{1}{3}\right)\frac{\left(3R^3-2R^2+3R\right)}{\left(2R^4+2\right)}$
	OSPRE [8]	$\frac{3}{2}\frac{R^2+R}{R^2+R+1.0}$
	Super-B [18]	$\max\left(0,\min\left(2R,1\right),\min\left(R,2\right)\right)$

3.0 SIMULATION DESCRIPTION

Hydrogen release from a square area of 10^{-4} m^2 was simulated. Hydrogen enters the domain at sonic conditions (i.e. 1292.1 m/s), with a vertical direction towards the ground. These parameters was

chosen because are usually met in high pressure hydrogen releases. The release point is located 0.1 m above the ground. There are not any obstacles in the domain.

3.1 Numerical details - Evaluation strategy

In order to evaluate the convective numerical schemes, four series of sensors were placed along arcs (semicircles) at 0.05, 0.10, 0.20 and 0.35 m from the source and at 0.005 m above the ground (Fig. 3). Each series has 41 sensors at equidistance angles. We chose to place the sensors in that configuration because hydrogen mass fraction and x-y velocity component should remain constant along a circle. The contour lines of these variables are also expected to have a circular geometry. The evaluation of the convective schemes is made by calculating the ratio of the biggest to the lowest value in a series of sensors. The closer to the unity this ratio is, the more appropriate the scheme is for the current problem.

In real scale hydrogen dispersion simulations it is a common practice to discretize the source using only one cell in order to keep the total number of cells in a reasonable number. As a result, a grid with one cell discretization of the source is first used in order to evaluate the numerical schemes. The size of this cell is equal to 0.01 x 0.01 x 0.01 m. Cells' dimensions is kept constant in a rectangular area (of length and width equal to 0.2 m) between the ground and the source. Far from the source the cells' size are expanded with an expansion factor of 1.12. The grid in the area around the source is shown in Fig. 3. Denser grids are also used in order to examine the grid independency of the results. Domain's dimensions are 2 x 2 x 0.3 m.

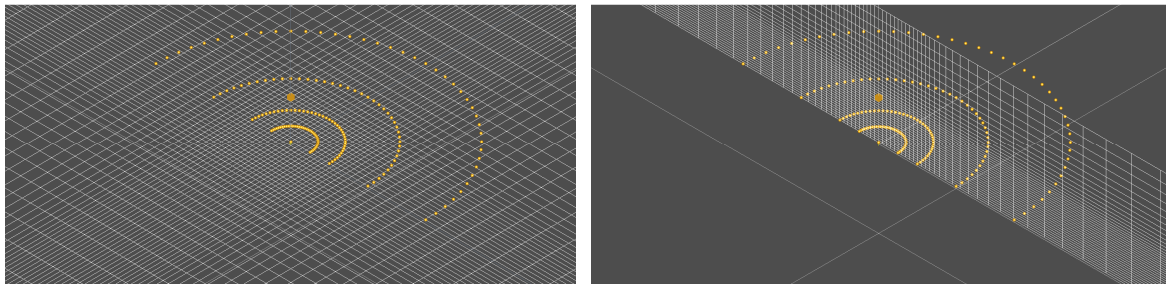

Figure 3. XY (left) and XZ (right) grid view for one cell discretization of the source. Sensor positions are represented by the orange spheres. Source position is at the bottom surface of the small cube at the center of the figures

In each simulation the same convective scheme is used in both Navier-Stokes equations and the conservation equation of hydrogen mass fraction. For the discretization of the temporal term first order backwards differences are used. Finally, the results are presented at the time of 1 sec when steady state is approached.

4.0 RESULTS AND DISCUSSION

4.1 One cell discretization of the source

In Fig. 4 and Fig. 5 the hydrogen mass fraction and the x-y velocity component contours (VELXY) at t=1 sec are presented for the convective schemes of Table 1 and for one cell discretization of the source. We observe that the contours of both hydrogen mass fraction and x-y velocity component have unphysical shapes for the majority of the convective schemes. A butterfly structure seems to exist in the majority of the schemes. The only scheme which seems to have a physical circular geometry is Fromm. In Fig. 6 and Fig. 7 hydrogen mass fraction and VELXY are shown respectively along the four semicircular sensor series. We observe that although prediction should be a straight line, it exhibits strong oscillations. In order to quantify the divergence from the straight line, we calculate the ratio of the maximum to the minimum value along each semicircle. The results are presented in Table 2 for the VELXY variable and in Table 3 for the hydrogen mass fraction. The results have been sorted in increasing order of the ratio at the first semicircle. We observe that the Fromm scheme gives the

best results among all schemes for both hydrogen mass fraction and VELXY. The MUSCL and the Cubic Upwind scheme produce the next best solutions. On the other hand the Upwind scheme gave the worst results. Similar results with Upwind gave the Super-B and the MinMod scheme.

Upwind

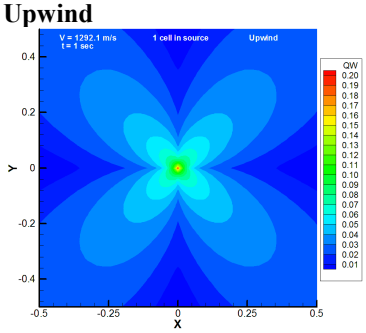

QUICK

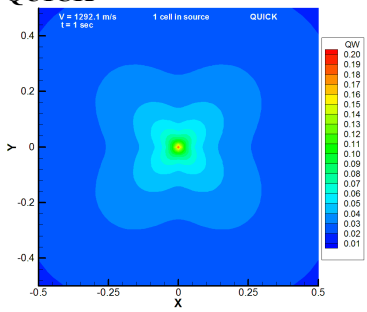

Fromm

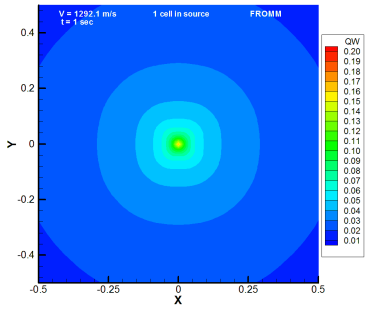

Cubic Upwind

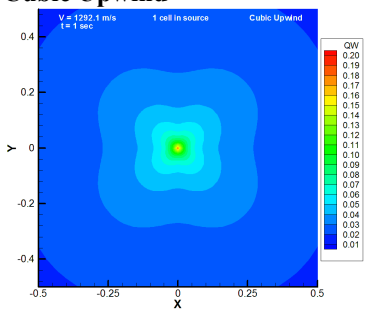

MUSCL

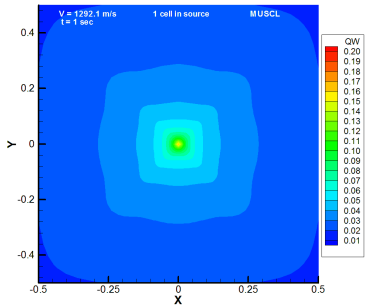

Van Leer

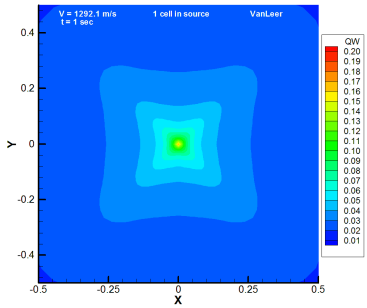

SMART

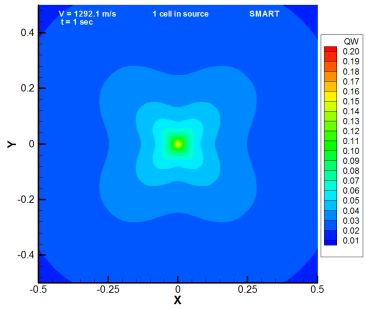

Bounded Central Differences

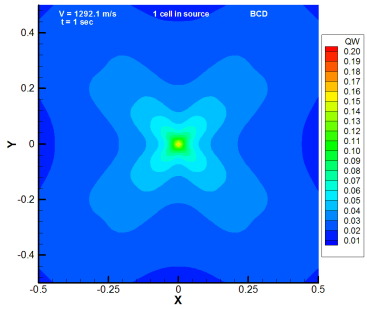

Super-B

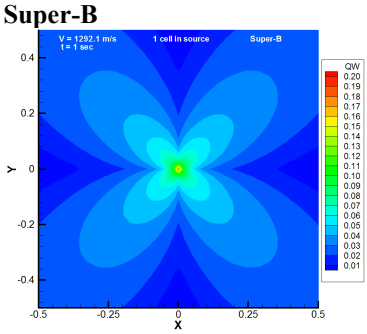

Koren-PR

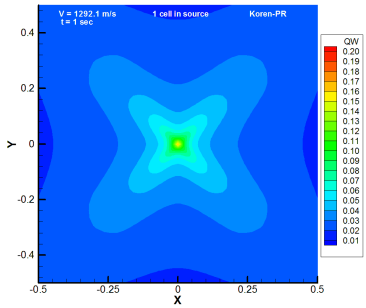

Spekreijse

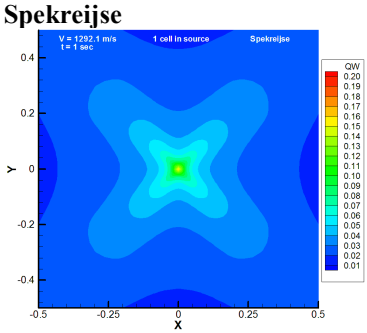

CHARM

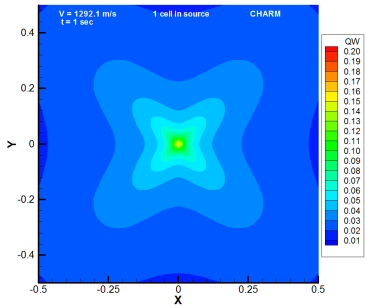

MinMod

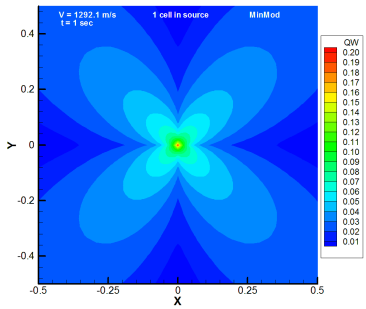

Van Albada

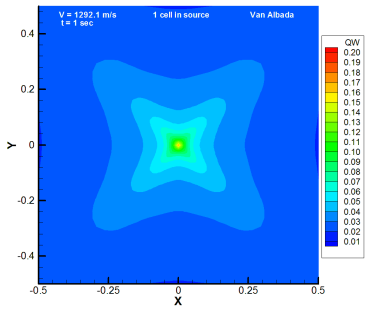

OSPRE

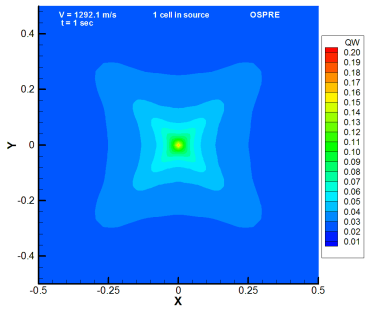

Figure 4. Hydrogen mass fraction contours at z=0.005 m plane at t = 1 sec - one cell discretization of the source

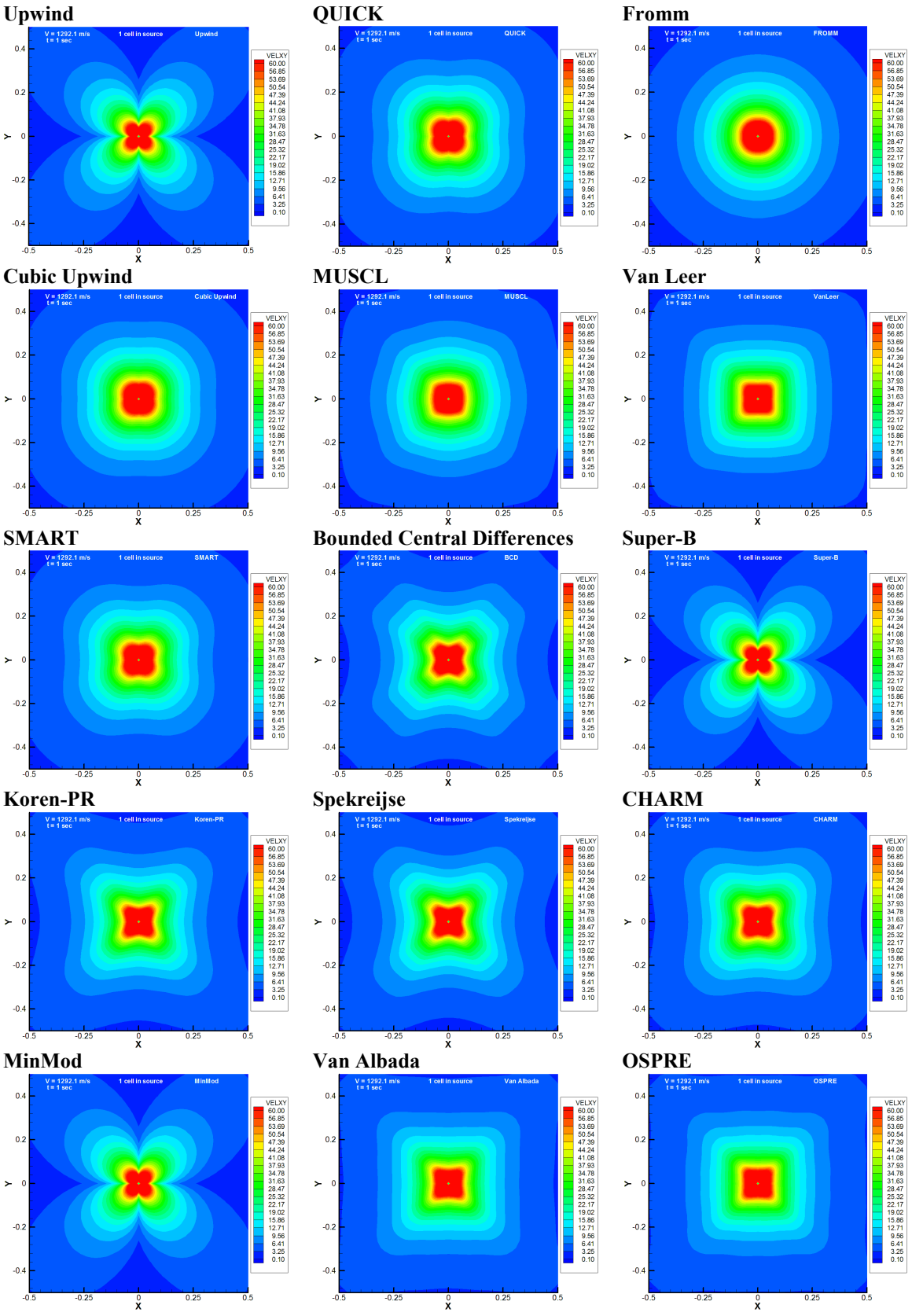

Figure 5. x-y velocity component (VELXY) contours at z=0.005 m plane at t = 1 sec - one cell discretization of the source

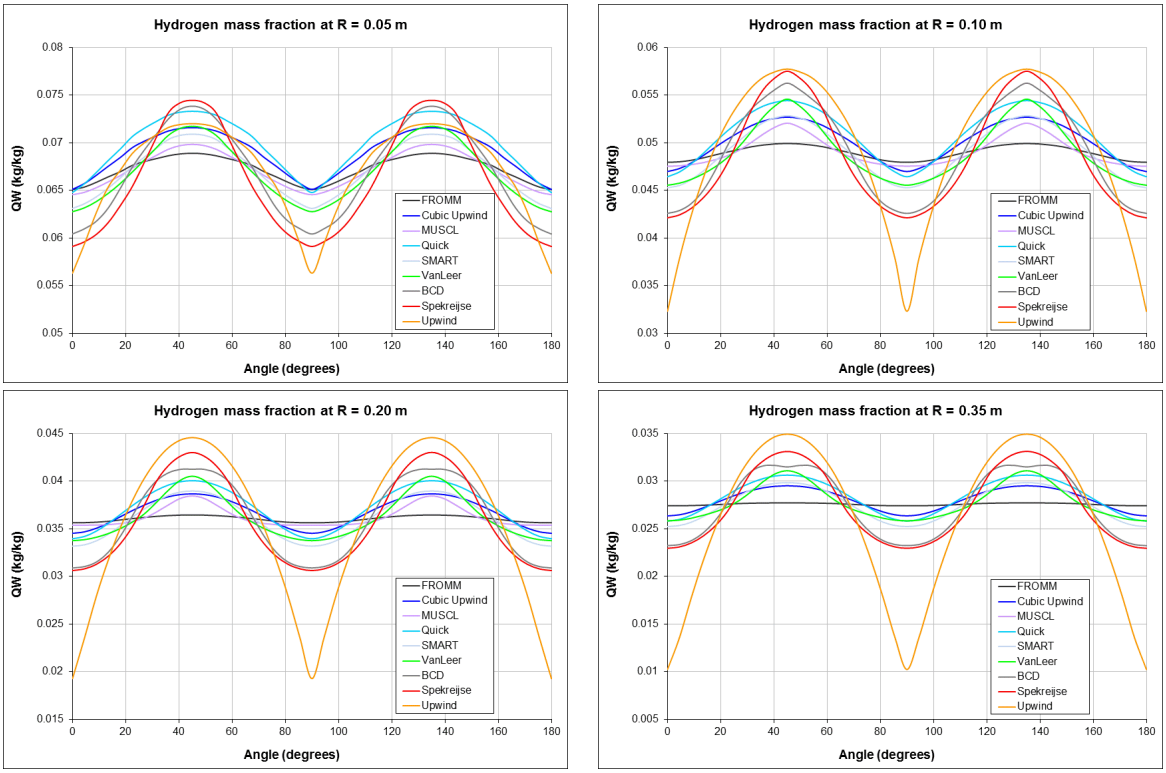

Figure 6. Hydrogen mass fraction at the four sensor series for ten of the convective schemes - one cell discretization of the source

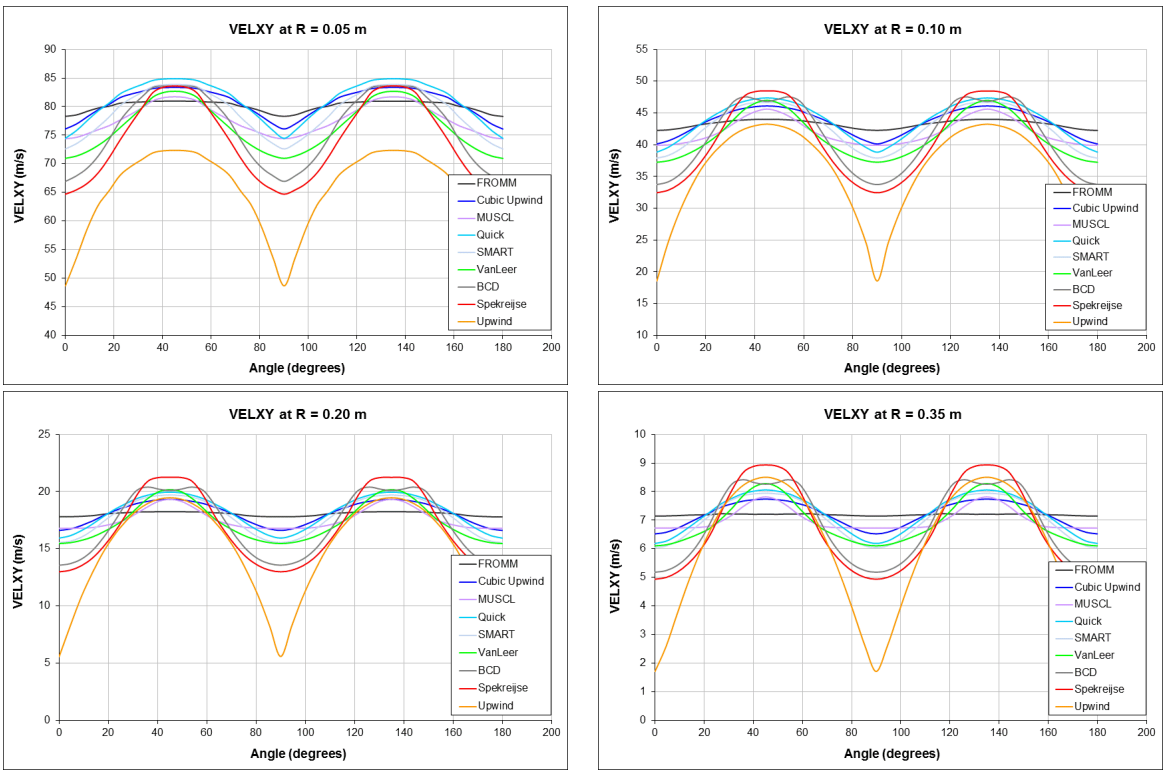

Figure 7. VELXY at the four sensor series for ten of the convective schemes - one cell discretization of the source

Table 2. Ratio of the maximum to the minimum hydrogen mass fraction value along each semicircle - one cell discretization of the source

Ratio of the maximum to the minimum hydrogen mass fraction				
Scheme	**R_1=0.05 m**	**R_2=0.10 m**	**R_3=0.20 m**	**R_4=0.35 m**
Fromm	1.059	1.041	1.023	1.011
MUSCL	1.082	1.095	1.087	1.162
Cubic Upwind	1.099	1.122	1.120	1.120
SMART	1.124	1.167	1.174	1.182
QUICK	1.132	1.172	1.180	1.187
Van Leer	1.143	1.198	1.200	1.204
OSPRE	1.170	1.249	1.256	1.266
Van Albada	1.202	1.294	1.309	1.324
CHARM	1.208	1.300	1.317	1.333
Bounded CD	1.222	1.321	1.335	1.362
Koren-PR	1.252	1.363	1.392	1.419
Spekreijse	1.260	1.365	1.405	1.443
Super-B	1.279	1.787	2.312	3.414
MinMod	1.279	1.787	2.312	3.414
Upwind	1.279	1.787	2.312	3.414

Table 3. Ratio of the maximum to the minimum VELXY value along each semicircle - one cell discretization of the source

Ratio of the maximum to the minimum VELXY				
Scheme	**R_1=0.05 m**	**R_2=0.10 m**	**R_3=0.20 m**	**R_4=0.35 m**
Fromm	1.034	1.041	1.025	1.011
Cubic Upwind	1.096	1.149	1.163	1.187
MUSCL	1.099	1.143	1.151	1.162
QUICK	1.140	1.220	1.252	1.302
SMART	1.156	1.231	1.268	1.315
Van Leer	1.165	1.262	1.305	1.357
OSPRE	1.205	1.333	1.397	1.477
Van Albada	1.235	1.389	1.472	1.576
CHARM	1.236	1.373	1.455	1.556
Bounded CD	1.249	1.409	1.503	1.624
Koren-PR	1.286	1.473	1.592	1.739
Spekreijse	1.293	1.494	1.636	1.809
Super-B	1.487	2.332	3.484	4.969
MinMod	1.487	2.332	3.484	4.969
Upwind	1.487	2.332	3.484	4.969

4.2 Four cells discretization of the source

In order to examine the grid effect on the results, the simulations are repeated using four cells to discretize the source. In Fig. 8 the hydrogen mass fraction contours at t=1 sec are depicted. We observe that the majority of the convective schemes have a physical shape of contours (near to circle). Upwind, Super-B and MidMod schemes have given again the worst results. However, even these cases are improved compared to the one cell discretization case. In Fig. 9 hydrogen mass fractions are shown along the four semicircular sensor series. The results have been improved significantly compared to the case with the one cell discretization. In order to quantify them we calculate the ratio of the maximum to the minimum value along each semicircle. The results are presented in Table 4. The results have been sorted in increasing order of the ratio at the first semicircle. The Fromm scheme gave the best results among all schemes. MUSCL and Van Leer schemes produce the next best solutions. Upwind, Super-B and MinMod scheme gave the worst results. Comparing the ratios of one cell discretization case (Table 2) with the ratios in four cells discretization case (Table 4), a great improvement in the ratio values is observed.

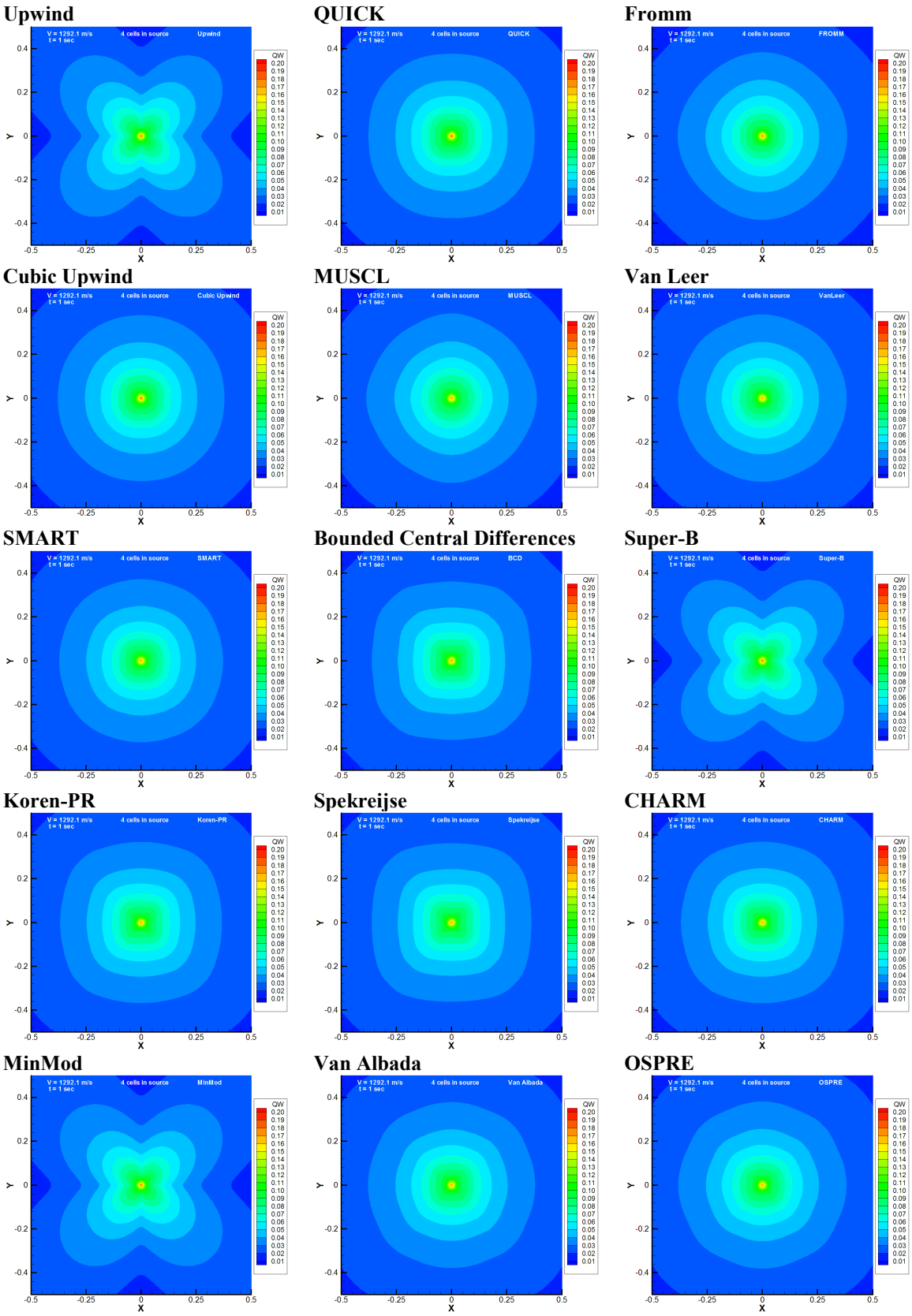

Figure 8. Hydrogen mass fraction contours at z=0.005 m plane at t = 1 sec - four cells discretization of the source

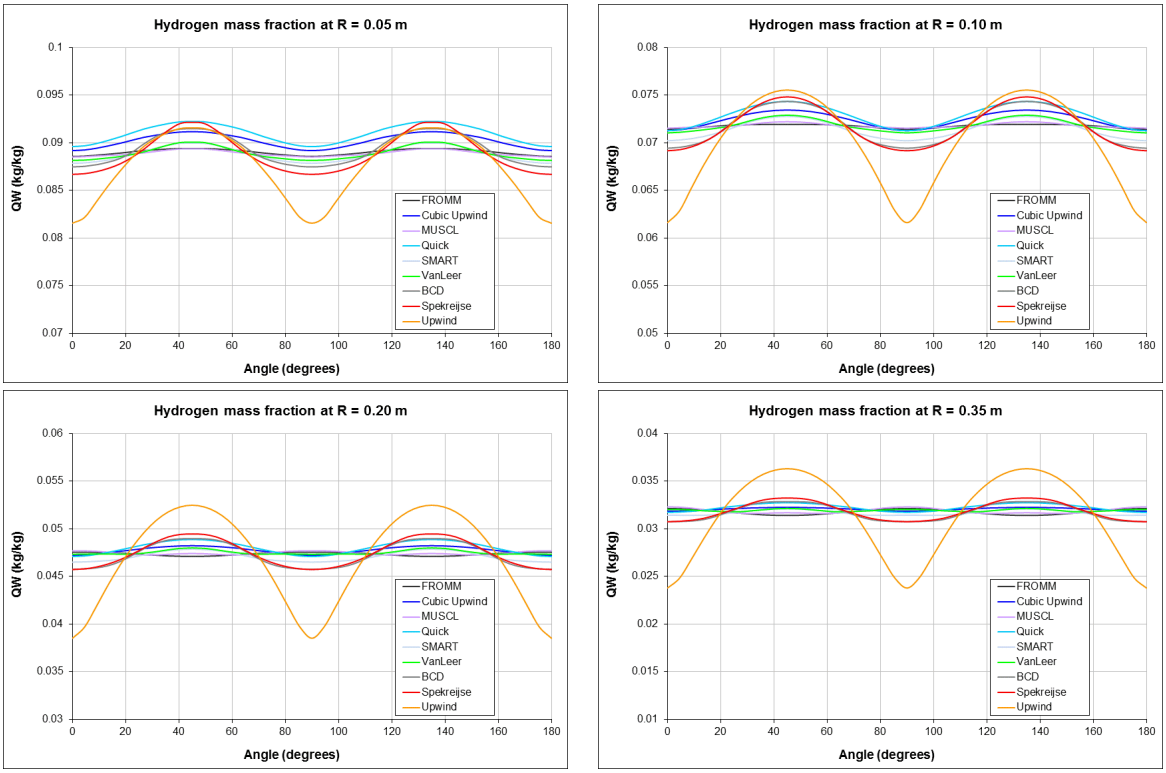

Figure 9. Hydrogen mass fraction at the four sensor series for ten of the convective schemes - four cells discretization of the source

Table 4. Ratio of the maximum to the minimum hydrogen mass fraction value along each semicircle - four cells discretization of the source

Ratio of the maximum to the minimum hydrogen mass fraction				
Scheme	**R_1=0.05 m**	**R_2=0.10 m**	**R_3=0.20 m**	**R_4=0.35 m**
Fromm	1.009	1.007	1.009	1.023
MUSCL	1.010	1.009	1.009	1.022
Van Leer	1.022	1.026	1.014	1.011
Cubic Upwind	1.022	1.030	1.021	1.013
SMART	1.024	1.036	1.029	1.021
OSPRE	1.027	1.033	1.024	1.021
QUICK	1.029	1.043	1.038	1.032
Van Albada	1.034	1.042	1.034	1.027
CHARM	1.038	1.053	1.049	1.044
Bounded CD	1.046	1.071	1.071	1.068
Koren-PR	1.050	1.066	1.063	1.059
Spekreijse	1.063	1.082	1.082	1.081
Super-B	1.123	1.226	1.362	1.527
MinMod	1.123	1.226	1.362	1.527
Upwind	1.123	1.226	1.362	1.527

4.3 Grid independency

In order to examine the impact of the grid on the results, simulations with denser grids were also carried out. The grid independency was performed for the Upwind scheme by using 9 equal-size cells for source discretization and for the MUSCL scheme by using 9 and 16 equal-size cells for source discretization. The size of the cells remains constant (and equal to the size of the cells in the source) at the area around the source as it is described in paragraph 3.1. In Fig. 10 the hydrogen contours are

presented. We observe that the Upwind scheme fails to achieve a grid independent solution. Even for a 9 cell discretization of the source the shape of the contours lines deviate from circular. However the butterfly structure seems to be smoothed out as the number of cells increases. The convergence to a grid independent solution seems to be very slow, probably because of the low order accuracy (1st order) of the Upwind scheme. On the other hand for the MUSCL scheme a near grid independent solution is achieved with the 9 cells discretization. Furthermore, a physical shape of the contours is achieved even with the 4 cells discretization.

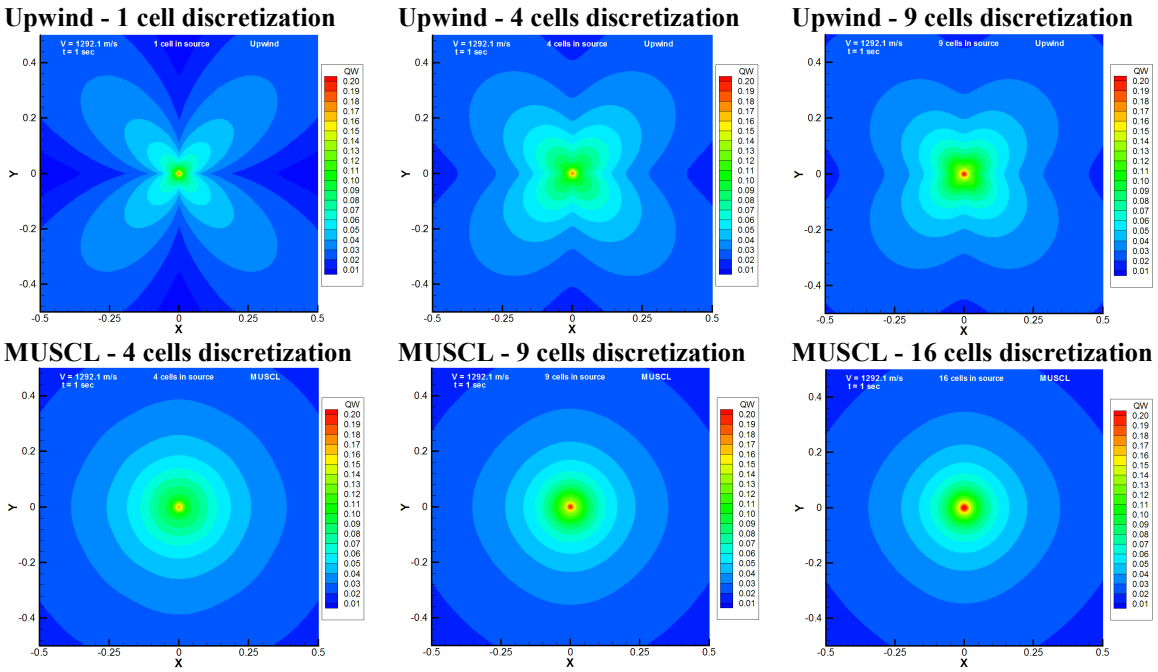

Figure 10. Hydrogen mass fraction contours at z=0.005 m plane at t = 1 sec for Upwind and MUSCL scheme for 1, 4 and 9 cells discretization of the source

5.0 CONCLUSIONS

A number of convective schemes were tested for the simulation of a hydrogen impinging jet. The shape of the contour lines of hydrogen mass fraction was examined. In the case of one cell discretization of the source, the only scheme which achieved a circular geometry of the contours is the Fromm scheme. When the number of cells increases, the performance of all schemes is improved. Nevertheless, Fromm scheme still produces the best results. The only schemes which failed to reproduce satisfactory results even in the case of the four-cell discretization are the Upwind, the MinMod and the Super-B. Finally, the grid independency study revealed that 9 cells discretization is sufficient to achieve a near grid independent solution for the MUSCL scheme whereas it is not for the Upwind scheme.

ACKNOWLEDGEMENTS

The authors would like to thank the Fuel Cell and Hydrogen Joint Undertaking for the co-funding of the project SUSANA (“SUpport to SAfety ANalysis of Hydrogen and Fuel Cell Technologies”, Grant agreement no: 325386).

REFERENCES

1. Zuckerman, N. and Lior, N., Jet Impingement Heat Transfer: Physics, Correlations, and Numerical Modeling, *Adv. Heat Transf.*, **39**, No. 6, 2006, pp. 565–631.
2. Friedrich, A., Grune, J., Kotchourko, N., Kotchourko, A., Sempert, K., Stern, G. and Kuznetsov, M., Experimental study of jet-formed hydrogen-air mixtures and pressure loads from their

deflagrations in low confined surroundings, Proceedings of 2nd International Conference on Hydrogen Safety, 2007.
3. Middha, P., Hansen, O.R., Grune, J. and Kotchourko, A., CFD calculations of gas leak dispersion and subsequent gas explosions: validation against ignited impinging hydrogen jet experiments., *J. Hazard. Mater.*, **179**, No. 1–3, 2010, pp. 84–94.
4. Schefer, R.W., Merilo, E.G., Groethe, M.A. and Houf, W.G., Experimental investigation of hydrogen jet fire mitigation by barrier walls, *Int. J. Hydrogen Energy*, **36**, No. 3, 2011, pp. 2530–2537.
5. Ranga Dinesh, K.K.J., Jiang, X. and van Oijen, J.A., Numerical simulation of hydrogen impinging jet flame using flamelet generated manifold reduction, *Int. J. Hydrogen Energy*, **37**, No. 5, 2012, pp. 4502–4515.
6. Mira Martinez, D. and Jiang, X., Numerical investigations of a hydrogen impinging flame with different finite-rate chemical kinetic mechanisms, *Fuel*, **109**, 2013, pp. 285–296.
7. Venetsanos, A.G., Papanikolaou, E. and Bartzis, J.G., The ADREA-HF CFD code for consequence assessment of hydrogen applications, *Int. J. Hydrogen Energy*, **35**, No. 8, 2010, pp. 3908–3918.
8. Waterson, N.P. and Deconinck, H., Design principles for bounded higher-order convection schemes – a unified approach, *J. Comput. Phys.*, **224**, No. 1, 2007, pp. 182–207.
9. Leonard, B.P., A stable and accurate convective modelling procedure based on quadratic upstream interpolation, *Comput. Methods Appl. Mech. Eng.*, **19**, No. 1, 1979, pp. 59–98.
10. Fromm, J.E., A method for reducing dispersion in convective difference schemes, *J. Comput. Phys.*, **3**, No. 2, 1968, pp. 176–189.
11. Agarwal, R.K., A third-order-accurate upwind scheme for Navier–Stokes solutions at high Reynolds numbers, in *19th AIAA Aerospace Sciences Meeting*, 1981, pp. 1981–112.
12. Zhu, J. and Rodi, W., A low dispersion and bounded convection scheme, *Comput. Methods Appl. Mech. Eng.*, **92**, No. 1, 1991, pp. 87–96.
13. Van Albada, G.D and Van Leer, B., A comparative study of computational methods in cosmic gas dynamics, *Astron. Astrophys*, **108**, 1982, pp. 76.
14. Van Leer, B., Towards the ultimate conservative difference scheme. II. Monotonicity and conservation combined in a second-order scheme, *J. Comput. Phys.*, **14**, No. 4, 1974, pp. 361–370.
15. Van Leer, B., Towards the ultimate conservative difference scheme. IV. A new approach to numerical convection, *J. Comput. Phys.*, **23**, No. 3, 1977, pp. 276–299.
16. Gaskell, P.H. and Lau, A.K.C., Curvature-compensated convective transport: SMART, A new boundedness- preserving transport algorithm, *Int. J. Numer. Methods Fluids*, **8**, No. 6, 1988, pp. 617–641.
17. Koren, B., Upwind discretization of the steady Navier-Stokes equations, *Int. J. Numer. Methods Fluids*, **11**, No. 1, 1990, pp. 99–117.
18. Roe, P.L., Some contributions to the modelling of discontinuous flows, *Large-Scale Comput. Fluid Mech.*, **1**, 1985, pp. 163–193.